Methane Activation

DOI: 10.1002/anie.201200015

Direct Conversion of Methane into Formaldehyde Mediated by $[Al_2O_3]^{\bullet+}$ at Room Temperature**

Zhe-Chen Wang, Nicolas Dietl, Robert Kretschmer, Jia-Bi Ma, Thomas Weiske, Maria Schlangen, and Helmut Schwarz**

Dedicated to Professor George A. Olah on the occasion of his 85th birthday

As the major component of natural gas, methane (CH_4) is mainly used as fuel for power generation and as a chemical feedstock for the industrial production of syngas. The selective functionalization of CH_4 to more valuable chemicals under environmentally benign and economically feasible conditions constitutes one of the major contemporary challenges in chemistry,[1] and value-added products include methanol (CH_3OH) and formaldehyde (CH_2O).[2] As one of the top 25 most-produced chemicals worldwide, the annual production of CH_2O amounts to more than 20 million tons per year,[3] and the major large-scale process is the conversion of CH_3OH at high temperature using iron- or silver-based catalysts, Reaction (1).[3]

$$2\,CH_3OH + O_2 \rightarrow 2\,CH_2O + 2\,H_2O \quad (1)$$

Currently, the industrial production of CH_2O starting from CH_4 proceeds in several steps and requires high pressure and high temperature, thus consuming a large amount of energy; further, the byproducts are harmful to the environment.[4] Despite extensive efforts, the direct conversion of CH_4 into CH_2O remains a great challenge[5] because formaldehyde is much more easily oxidized than methane.[3] To date, no commercial catalyst is available (even at high temperature) for the one-step conversion $CH_4 \rightarrow CH_2O$ with acceptable yields, a result of the interdependence of conversion and selectivity.[4b,6]

As has been demonstrated, CH_4 can be activated catalytically with unexpected low activation energies,[7] and reactive Al–O Lewis acid/Lewis-base pairs are found to act as the key species on the (110) face of γ-Al_2O_3.[8] One efficient approach to improve the performance of existing catalysts is to understand the detailed mechanisms by which single-site catalysts operate. This understanding can ideally be achieved by gas-phase studies in which models of the active site are prepared, mass-selected, and studied under (near) single-collision conditions in their reactions with various substrates.[9] Sierka et al. reported the unexpected structure of $[(Al_2O_3)_4]^{\bullet+}$ which has a terminal Al–O$^{\bullet}$ single bond by using gas-phase infrared-photodissociation spectroscopy,[10] and reactivity studies revealed that $[(Al_2O_3)_x]^{\bullet+}$ clusters ($x = 3$, 4, 5) engage in H-atom abstraction from methane under thermal conditions;[11] this reactivity pattern can be explained by the spin density located at terminal oxygen atoms which turned out to be crucial for hydrogen-atom transfer (HAT) processes.[2,9a,12]

In previous studies, different types of methane activation by gaseous oxide clusters have been described,[2,9,12f,h,13] including HAT, oxygen-atom transfer, carbene as well as formaldehyde formation [Eq. (2)–(5)].

$$[(M_xO_y)O]^+ + CH_4 \rightarrow [(M_xO_y)OH]^+ + CH_3^{\bullet} \quad (2)$$

$$[(M_xO_y)O]^+ + CH_4 \rightarrow [M_xO_y]^+ + CH_3OH \quad (3)$$

$$[(M_xO_y)O]^+ + CH_4 \rightarrow [(M_xO_y)CH_2]^+ + H_2O \quad (4)$$

$$[(M_xO_y)O]^+ + CH_4 \rightarrow [M_xO_yH_2]^+ + CH_2O \quad (5)$$

Reaction (3) is the gas-phase analogue of the formation of methanol from methane. Formaldehyde can be generated under these conditions by the rarely observed direct oxidation of CH_4, Reaction (5), and $[PtO_2]^+$ and $[CrO_2]^+$ have been reported to bring about this conversion; however, the chemoselectivity is with 2% and 30%, respectively, rather poor.[13j,k] Herein, we show that this direct oxidation is possible with good chemoselectivity in the reaction of gaseous $[Al_2O_3]^{\bullet+}$ clusters with CH_4 at room temperature.

Figure 1 shows the thermal reactions of mass-selected $[Al_2O_3]^{\bullet+}$ with CH_4, CD_4, and CH_2D_2, at a pressure of $8\times$

[*] Dr. Z.-C. Wang, Dipl.-Chem. N. Dietl, Dipl.-Chem. R. Kretschmer, J.-B. Ma, Dr. T. Weiske, Dr. M. Schlangen, Prof. Dr. H. Schwarz
Institut für Chemie, Technische Universität Berlin
Strasse des 17. Juni 135, 10623 Berlin (Germany)
E-mail: maria.schlangen@mail.chem.tu-berlin.de
helmut.schwarz@mail.chem.tu-berlin.de
Prof. Dr. H. Schwarz
Chemistry Department, Faculty of Science
King Abdulaziz University
Jeddah 21589 (Saudi Arabia)
E-mail: hschwarz@kau.edu.sa
Dr. Z.-C. Wang
Department of Chemistry, Colorado State University
Fort Collins, CO 80523-1872 (USA)

[**] This work is supported by the Fonds der Chemischen Industrie, the Deutsche Forschungsgemeinschaft (DFG), and the Cluster of Excellence "Unifying Concepts in Catalysis" (coordinated by the Technische Universität Berlin and funded by the DFG). For computational resources, the Institut für Mathematik at the Technische Universität Berlin is acknowledged. Z.-C.W. is grateful to the Alexander von Humboldt Stiftung for a postdoctoral fellowship. R.K. acknowledges the Stiftung Stipendien-Fonds des Verbandes der Chemischen Industrie for a Kékulé scholarship. We thank Dr. Jianwen Liu (Humboldt Universität zu Berlin) for helpful discussions.

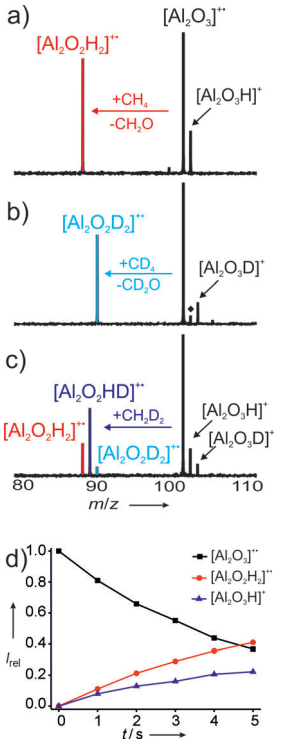

Figure 1. Mass spectra showing the reactions of $[Al_2O_3]^{\bullet+}$ clusters with CH_4 (a), CD_4 (b), and CH_2D_2 (c) at a pressure of 8×10^{-9} mbar and a reaction delay of 4 s. The relative intensities of the reactant ion $[Al_2O_3]^{\bullet+}$ as well as the product ions $[Al_2O_3H]^+$ and $[Al_2O_3H_2]^{\bullet+}$ in the reaction with CH_4 as a function of time are shown in (d). The signal marked with ◆ in (b) is caused by HAT from background impurities, such as water or other residual hydrocarbons.

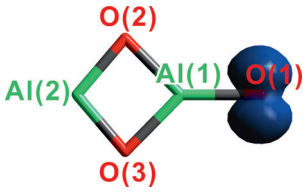

Figure 2. Optimized ground-state structure of $[Al_2O_3]^{\bullet+}$ (**1**) (C_{2v}) as revealed by DFT calculations; the blue iso-surface indicates the spin-density distribution.

10^{-9} mbar, respectively. Not entirely unexpected, HAT takes place, resulting in the formation of $[Al_2O_3X]^+$ (X = H, D). In analogy to the related $[(Al_2O_3)_x]^{\bullet+}$ (x = 3,4,5)/CH_4 systems,[11] the ground state of $[Al_2O_3]^{\bullet+}$ has a high spin density at a terminal oxygen atom (Figure 2) being beneficial for HAT.[12b] Furthermore, density-functional theory (DFT) calculations predict Reaction (6) to be exothermic by −1.03 eV (ΔE = zero-point vibrational-energy corrected reaction energy). However, Reaction (6) takes place with a branching ratio of only 35%; the main reaction channel corresponds to the generation of $[Al_2O_2H_2]^{\bullet+}$ by evaporation of neutral CH_2O according to Reaction (7).

$$[Al_2O_3]^{\bullet+} + CH_4 \rightarrow [Al_2O_3H]^+ + CH_3^{\bullet},\ \Delta E = -1.03\ \text{eV}\ 35\% \quad (6)$$

$$[Al_2O_3]^{\bullet+} + CH_4 \rightarrow [Al_2O_2H_2]^{\bullet+} + CH_2O,\ \Delta E = -2.34\ \text{eV}\ 65\% \quad (7)$$

All the reactions are confirmed by labeling experiments with CD_4 in which $[Al_2O_2D_2]^{\bullet+}$ is generated (Figure 1 b). The slope of the time dependency of generating $[Al_2O_2H_2]^{\bullet+}$ suggests that $[Al_2O_2H_2]^{\bullet+}$ is a primary reaction product; Figure 1 d. The direct formation of $[Al_2O_2H_2]^{\bullet+}$ is further supported by double resonance experiments;[14] they demonstrate that the intensity of $[Al_2O_2H_2]^{\bullet+}$ is not affected when the HAT product $[Al_2O_3H]^+$ is continuously ejected from the reaction cell. Thus $[Al_2O_3H]^+$ does not serve as a precursor. The intensity ratio of the isotopic products $[Al_2O_2H_2]^{\bullet+}$:$[Al_2O_2HD]^{\bullet+}$:$[Al_2O_2D_2]^{\bullet+}$ in the reaction of $[Al_2O_3]^{\bullet+}$ with CH_2D_2 is to 1.00:2.18:0.22 (Figure 1 c); considering a kinetic isotopic effect (KIE) of 1.8 as determined for the first HAT, this branching ratio can be reproduced resulting in a relatively good agreement (1:2.11:0.28) when a KIE of 2.0 is assumed for the second C–H(D) bond activation.[15] The rate constant $k([Al_2O_3]^{\bullet+} + CH_4)$ is 7.0×10^{-11} cm^3 s^{-1} molecule^{-1} with ±30% uncertainty; this corresponds to an efficiency of around 7%, relative to the collision rate.[16]

To obtain mechanistic insight into the $CH_4 \rightarrow CH_2O$ oxidation mediated by $[Al_2O_3]^{\bullet+}$, we carried out DFT calculations. The corresponding potential-energy surfaces (PESs) of this reaction are shown in Figure 3. The most stable structure of the reactant cation $[Al_2O_3]^{\bullet+}$ (**1**) corresponds to a four-membered, planar Al-O-Al-O ring with one of the Al atoms (denoted as Al(1)) bearing a terminal oxygen atom at which the unpaired electron is located (Figure 2). During geometry optimization of the $[Al_2O_3]^{\bullet+}/CH_4$ encounter complex, in a barrier-free process the methanol complex $[Al_2O_2(HOCH_3)]^{\bullet+}$ (**2**) is directly formed by insertion of the terminal oxygen (denoted as O(1)) into the C–H(1) bond of methane; this process is shown in detail in Figure 4. A remarkably large amount of energy (ΔE = −3.12 eV) is gained in this reaction step; in contrast to the related $[(Al_2O_3)_4]^{\bullet+}/CH_4^{\bullet}$ system,[11] an $[Al_2O_3H]^+ \cdot CH_3$ complex in which the methyl radical is loosely bound to the newly formed hydroxy group cannot be located on the PES as a local minimum.

From intermediate **2**, formation of the product pairs $[Al_2O_3H]^+$ (**7**)/$CH_3^{\bullet}$ [Reaction (6)], or $[Al_2O_2]^{\bullet+}$ (**8**)/CH_3OH [Reaction (8)], is thermodynamically possible via cleavage of the O(1)–C or Al(1)–O(1) bonds, respectively (Figure 3 a). However, complete oxygen-atom transfer to produce CH_3OH [Reaction (8)], is energetically much less favored when compared to Reactions (6) and (7); this may explain why $[Al_2O_2]^{\bullet+}$ is not detected experimentally.

$$[Al_2O_3]^{\bullet+} + CH_4 \rightarrow [Al_2O_2]^{\bullet+} + CH_3OH,\ \Delta E = -0.29\ \text{eV} \quad (8)$$

In line with the experimental findings, Reaction (7) corresponds to the thermodynamically most favorable channel when compared to Reactions (6) and (8). However, this pathway requires a rather complex reaction sequence mechanistically.

As to the generation of CH_2O, after formation of **2** the O(1)–H(1) bond is cleaved and a μ-hydroxy ligand is formed by the sequence **2**→**TS2/3**→**3** (Figure 3 a). A Mulliken atomic-spin density (MASD) analysis indicates that the spin is mainly localized on the less-coordinated Al(2) atom in **2**, **3**,

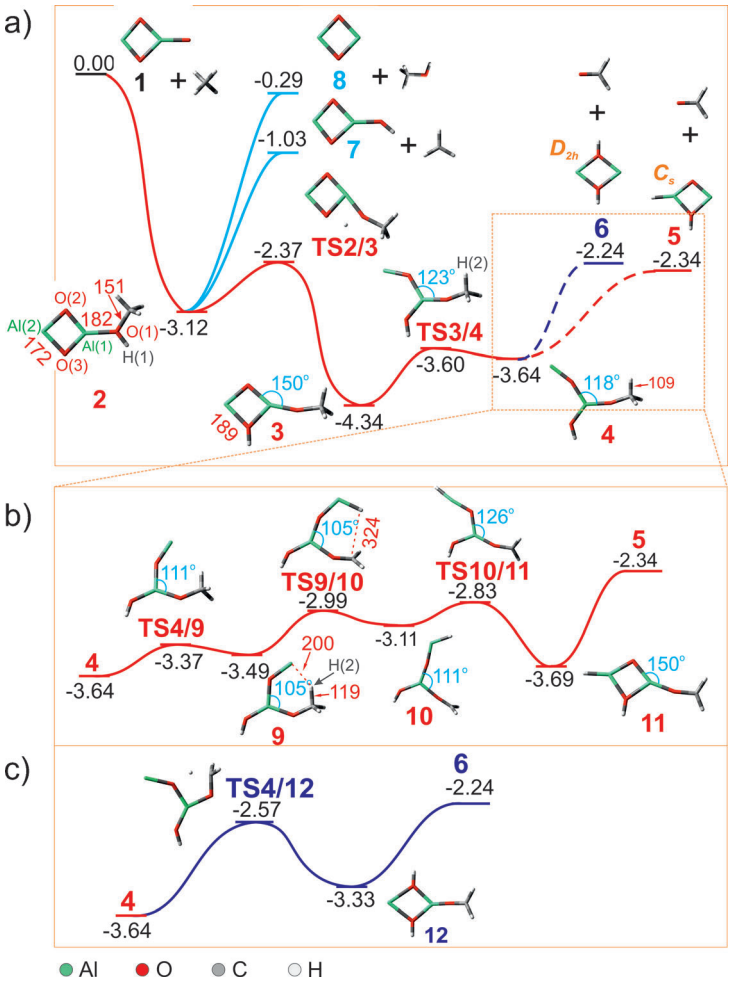

Figure 3. The PESs for the reaction of $[Al_2O_3]^{\bullet+}$ with CH_4. An overview of the reaction (a); detailed reaction sequences from intermediate **4** to the products **5** and **6** (b) and (c), respectively. The energy values [eV] are relative to the entrance channel and corrected for zero-point vibrational energies. Some key bond lengths [pm] and angles [°] are given in red and blue, respectively.

as well as in **TS2/3** (0.85 μB, 0.89 μB, and 0.86 μB, respectively), with no spin distribution at the hydrogen and oxygen atoms. The following step **3**→**TS3/4**→**4** involves the cleavage of the Al(2)–O(3) bond which had already been elongated from 172 pm in **2** to 189 pm in **3**. For the formation of CH_2O from **4**, two alternative pathways are accessible under thermal conditions (Figure 3b,c). The pathway given in red in Figure 3b, leads eventually to the formation of product ion **5** ($[H\text{-}Al\text{-}\mu\text{-}O,\mu\text{-}(OH)\text{-}Al]^{\bullet+}$ (C_s)) and CH_2O. Crucial is intermediate **9** which has to accept a hydrogen atom from the CH_3O group of **4**. To this end, the angle ∡O(1)-Al(1)-O(2) decreases from 118° in **4** to 105° in **9**, thus moving the terminal aluminum atom Al(2) (MASD value of 0.89 μB) closer to the methyl group of the methoxy moiety. Note that owing to the proximity of the Al(2) atom, the C–H(2) bond in **9** is activated to a length of 119 pm, compared to the corresponding C–H bond length of 109 pm in **4**; the Al(2)–H(2) bond length in **9** is 200 pm. Next, this shortening enables the abstraction of H(2) by the pathway **9**→**TS9/10**→**10**; in **TS9/10**, the C–H(2) bond is already completely cleaved (C···H(2) 324 pm), and the ligand formaldehyde is formed accordingly. The C–O bond length of 122 pm in **TS9/10** is slightly shorter than the 125 pm in intermediate **6** owing to the preferred linear arrangement in **6** (∡Al-O-C 143° and 172° in **TS9/10** and **10**, respectively); both bond lengths are similar to the C–O bond length of 120 pm in free CH_2O. Intermediate **10**, prior to the liberation of CH_2O, undergoes a ring-closing rearrangement to intermediate **11** (**10**→**TS10/11**→**11**).

The alternative, direct elimination of CH_2O from **10** to produce the linear $[H\text{-}Al\text{-}O\text{-}Al\text{-}OH)]^{\bullet+}$ isomer (not shown in Figure 3) requires 0.88 eV more energy than the formation of **5**. In contrast to **10**, the C–O bond length of 136 pm in **11** almost corresponds to the bond length calculated for the C–O single bond in free CH_3OH (142 pm); finally, the MASD is fully localized at the C atom. Thus, although formaldehyde is less preformed in intermediate **11** than in **10**, its direct liberation from **10** is more demanding energetically.

The products $[Al\text{-}\mu(OH)_2\text{-}Al]^{\bullet+}$ (D_{2h}) (**6**) and CH_2O, which are only 0.1 eV higher in energy than **5** + CH_2O, are formed in the alternative pathway **4**→**TS4/12**→**12**→**6** (Figure 3c). In the reaction sequence to form **6**, HAT from the methyl group to the O(2) atom can take place directly from **4** via **TS4/12**. The four-membered ring is regenerated in intermediate **12** concomitant with the formation of a CH_2O ligand. Note that the energetically most demanding transition structures of both pathways, starting from **4**, are lower in energy than **TS2/3**; thus, formation of **6**, that is, $[Al_2O_2H_2]^{\bullet+}$ (D_{2h}), may well compete with that of **5** ($[Al_2O_2H_2]^{\bullet+}$ (C_s)) although **TS4/12** is 0.26 eV higher in energy than **TS6/7**.

The simplified PESs depicted in Figure 3 can well explain the experimental findings; nevertheless, the assignment of formaldehyde as the neutral molecule liberated in Reaction (7) is not absolutely unambiguous because the net formula of $[C,H_2,O]$ might also correspond to the formation of syngas, that is, CO and H_2 [Reaction (9)] and the experimental set-up does not permit the identification neutral molecules formed.

$$[Al_2O_3]^{\bullet+} + CH_4 \rightarrow [Al_2O_2H_2]^{\bullet+} + H_2 + CO,\ \Delta E = -2.30\,eV \qquad (9)$$

Although the computed thermochemistry of Reactions (9) and (7) are comparable, we nevertheless rule out Reaction (9) for the following reasons: 1) there are no experimental indications for the generation of intermediates $[Al_2O_2H_2(H_2)]^{\bullet+}$ or $[Al_2O_2H_2(CO)]^{\bullet+}$ required for the elimination of CO and H_2, respectively; 2) double-resonance experiments[14] on putative $[Al_2O_2H_2(H_2)]^{\bullet+}$ or $[Al_2O_2H_2(CO)]^{\bullet+}$ species do not affect the production of $[Al_2O_2H_2]^{\bullet+}$ (see Supporting Information Figure S1); 3) DFT calculations indicate that the transition structures for the formation of H_2 or the activation of a third C–H bond (necessary for CO formation), require significantly more energy than the CH_2O formation, see Figure 5.

In conclusion, the direct methane→formaldehyde conversion at room temperature can be brought about by the gas-

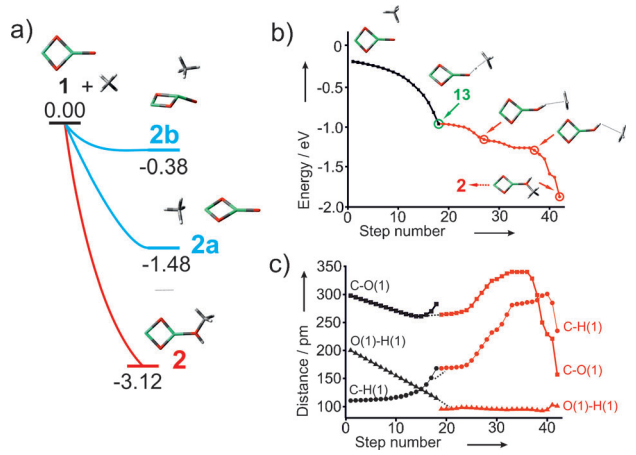

Figure 4. Detailed steps for the direct formation of the $[Al_2O_2(HOCH_3)]^+$ complex **2**. a) Competing processes for the formation of isomeric $[Al_2O_3]^{\bullet+}/CH_4$ encounter complexes. b) Black line: relaxed scan of the O(1)–H(1) distance from the reactants $[Al_2O_3]^{\bullet+} + CH_4$ to form structure **13**, $[Al_2O_3H]^+ \cdot CH_3$; red line: geometry optimization to convert **13** into intermediate **2**, $[Al_2O_2(HOCH_3)]^+$. In contrast to **2**, intermediate **13** does not correspond to a local minimum on the PES. c) Evolution of the C–O(1), O(1)–H(1), and C–H(1) bonds during the formation of **2**; black line: fixed scan of the O(1)–H(1) distance; red line: geometry optimization for the process **13**→**2**.

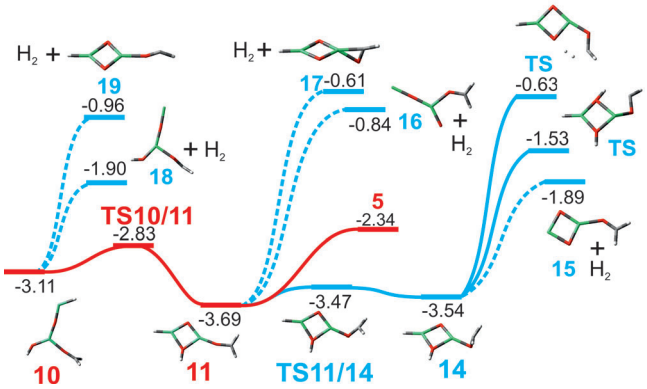

Figure 5. Possible product ions generated by the elimination of H_2 from intermediates **10**, **11**, or **14**, respectively; transition structures (**TS**) correspond to the C–H bond activation step necessary for the formation of CO. All alternative reaction paths require more energy as compared to the formation of **5**, that is, CH_2O elimination. The energies [eV] are given relative to the $[Al_2O_3]^{\bullet+}/CH_4$ entrance channel.

phase cluster cation $[Al_2O_3]^{\bullet+}$ through a complex mechanism involving both oxygen-atom and double hydrogen-atom transfers. After initial bond activation by insertion of the terminal oxygen atom from the $[Al_2O_3]^{\bullet+}$ cluster **1** into the C–H bond of methane, the transfer of a hydrogen atom to a distal site of the cluster initiates a sequence of ring-opening, hydrogen-atom transfer, and ring-closing of the Al-O-Al-O motif, all associated with rather low kinetic barriers, thus making the elimination of CH_2O more favorable than the simple HAT reaction channel. The suggested mechanism may shed light on the catalytic processes on the surfaces of real catalysts and may thus be used in the design of new or improving existing catalysts.

Experimental Section

The ion/molecule reactions were performed with a Spectrospin CMS 47X FTICR-mass spectrometer equipped with an external ion source as described elsewhere.[17] In brief, cluster cation $[Al_2O_7]^{\bullet+}$ is generated by laser ablation of an aluminum target using a Nd:YAG laser operating at 1064 nm in the presence of ca. 1% O_2 seeded in helium carrier gas. Using a series of potentials and ion lenses, the ions are transferred into the ICR cell which is positioned in the bore of a 7.05 T superconducting magnet. After excitation by radio-frequency radiation in the ion-cyclotron resonance (ICR) cell, $[Al_2O_7]^{\bullet+}$ dissociates by collisions with argon under the loss of two O_2 molecules to generate $[Al_2O_3]^{\bullet+}$.[12a] After further collisional thermalization, mass-selected $[Al_2O_3]^{\bullet+}$ is then treated with CH_4 under thermal conditions by introducing the reactant through a leak valve at stationary pressures. The experimental second-order rate constants are evaluated assuming the pseudo-first-order kinetic approximation after calibration of the measured pressure and acknowledgment of the ion-gauge sensitivities with an uncertainty of ±30%.[18] For the thermalized cluster ions a temperature of 298 K is assumed.[18]

The DFT calculations have been carried out using the Gaussian 09 program[19] employing the hybrid B3LYP exchange-correlation functional[20] with the unrestricted Kohn–Sham solution[21] and TZVP basis sets.[22] The unrestricted B3LYP/TZVP level of theory proved reliable in previous studies of $[(Al_2O_3)_x]^{\bullet+}$ ($x = 3,4,5$),[11] $[AlVO_4]^{\bullet+}$,[13d,23] $[AlVO_5]^{\bullet-}$,[24] and $[Al_2O_7]^{\bullet+}$[12a] and their gas-phase reactions with small hydrocarbons. For the optimization of transition structures (TS), we employed either the Berny algorithm[25] or the synchronous transit-guided quasi-Newton (STQN) method.[26] For most cases, initial approximate structures of the transition structures were obtained by relaxed potential-energy surface (PES) scans using an appropriate internal coordinate. Vibrational frequencies were calculated to characterize the nature of the stationary points as minima or transition structures; the relative energies (given in eV) were corrected for zero-point energy (ZPE) contributions. Intrinsic reaction-coordinate (IRC) calculations[27] were also performed to connect the TS with the local minima.

Received: January 2, 2012
Published online: March 1, 2012

Keywords: density functional calculations · gas-phase reactions · mass spectrometry · radical ions · reaction mechanisms

[1] a) J. R. Webb, T. Bolaño, T. B. Gunnoe, *ChemSusChem* **2011**, *4*, 37; b) G. A. Olah, A. Goeppert, G. K. S. Prakash, *Beyond Oil and Gas: The Methanol Economy*, Wiley-VCH, Weinheim, **2009**.
[2] D. Schröder, H. Schwarz, *Proc. Natl. Acad. Sci. USA* **2008**, *105*, 18114.
[3] G. Reuss, W. Disteldorf, A. O. Gamer, A. Hilt, "*Formaldehyde*" *in Ullmann's Encyclopedia of Industrial Chemistry*, Wiley-VCH, Weinheim, **2002**.
[4] a) G. A. Du, S. Y. Lim, Y. H. Yang, C. Wang, L. Pfefferle, G. L. Haller, *Appl. Catal. A* **2006**, *302*, 48; b) H. Berndt, A. Martin, A. Brückner, E. Schreier, D. Müller, H. Kosslick, G. U. Wolf, B. Lücke, *J. Catal.* **2000**, *191*, 384.
[5] H. Matsumura, K. Okumura, T. Shimamura, N. Ikenaga, T. Miyake, T. Suzuki, *J. Mol. Catal. A* **2006**, *250*, 122.
[6] D. L. An, Q. H. Zhang, Y. Wang, *Catal. Today* **2010**, *157*, 143.
[7] J. G. Larson, W. K. Hall, *J. Phys. Chem.* **1965**, *69*, 3080.
[8] a) R. Wischert, C. Copéret, F. Delbecq, P. Sautet, *Angew. Chem.* **2011**, *123*, 3260; *Angew. Chem. Int. Ed.* **2011**, *50*, 3202; b) C. Copéret, *Chem. Rev.* **2010**, *110*, 656.
[9] a) H. Schwarz, *Angew. Chem.* **2011**, *123*, 10276; *Angew. Chem. Int. Ed.* **2011**, *50*, 10096; b) M. Schlangen, H. Schwarz, *J. Catal.*

2011, *284*, 126; c) D. K. Böhme, H. Schwarz, *Angew. Chem.* **2005**, *117*, 2388; *Angew. Chem. Int. Ed.* **2005**, *44*, 2336.
[10] M. Sierka, J. Döbler, J. Sauer, G. Santambrogio, M. Brummer, L. Woste, E. Janssens, G. Meijer, K. R. Asmis, *Angew. Chem.* **2007**, *119*, 3437; *Angew. Chem. Int. Ed.* **2007**, *46*, 3372.
[11] S. Feyel, J. Döbler, R. Höckendorf, M. K. Beyer, J. Sauer, H. Schwarz, *Angew. Chem.* **2008**, *120*, 1972; *Angew. Chem. Int. Ed.* **2008**, *47*, 1946.
[12] a) N. Dietl, M. Schlangen, H. Schwarz, *Angew. Chem.* **2012**, DOI: 10.1002/ange.201108363; *Angew. Chem. Int. Ed.* **2012**, DOI: 10.1002/anie.201108363; b) Z.-C. Wang, T. Weiske, R. Kretschmer, M. Schlangen, M. Kaupp, H. Schwarz, *J. Am. Chem. Soc.* **2011**, *133*, 16930; c) K. Chen, Z.-C. Wang, M. Schlangen, Y.-D. Wu, X. Zhang, H. Schwarz, *Chem. Eur. J.* **2011**, *17*, 9619; d) A. Božović, S. Feil, G. K. Koyanagi, A. A. Viggiano, X. Zhang, M. Schlangen, H. Schwarz, D. K. Bohme, *Chem. Eur. J.* **2010**, *16*, 11605; e) M. Schlangen, H. Schwarz, *Dalton Trans.* **2009**, *46*, 10155; f) S. Feyel, J. Döbler, D. Schröder, J. Sauer, H. Schwarz, *Angew. Chem.* **2006**, *118*, 4797; *Angew. Chem. Int. Ed.* **2006**, *45*, 4681; g) I. Kretzschmar, A. Fiedler, J. N. Harvey, D. Schröder, H. Schwarz, *J. Phys. Chem. A* **1997**, *101*, 6252; h) D. Schröder, A. Fiedler, J. Hrušák, H. Schwarz, *J. Am. Chem. Soc.* **1992**, *114*, 1215.
[13] a) N. Dietl, C. van der Linde, M. Schlangen, M. K. Beyer, H. Schwarz, *Angew. Chem.* **2011**, *123*, 5068; *Angew. Chem. Int. Ed.* **2011**, *50*, 4966; b) N. Dietl, R. F. Höckendorf, M. Schlangen, M. Lerch, M. K. Beyer, H. Schwarz, *Angew. Chem.* **2011**, *123*, 1466; *Angew. Chem. Int. Ed.* **2011**, *50*, 1430; c) Y.-X. Zhao, X.-N. Wu, Z.-C. Wang, S.-G. He, X.-L. Ding, *Chem. Commun.* **2010**, *46*, 1736; d) Z.-C. Wang, X.-N. Wu, Y.-X. Zhao, J.-B. Ma, X.-L. Ding, S.-G. He, *Chem. Phys. Lett.* **2010**, *489*, 25; e) J.-B. Ma, X.-N. Wu, Y.-X. Zhao, X.-L. Ding, S.-G. He, *Phys. Chem. Chem. Phys.* **2010**, *12*, 12223; f) J. Roithová, D. Schröder, *Chem. Rev.* **2010**, *110*, 1170; g) A. Božović, S. Feil, G. K. Koyanagi, A. A. Viggiano, X. Zhang, M. Schlangen, H. Schwarz, D. K. Bohme, *Chem. Eur. J.* **2010**, *16*, 11605; h) G. de Petris, A. Troiani, M. Rosi, G. Angelini, O. Ursini, *Chem. Eur. J.* **2009**, *15*, 4248; i) D. Schröder, J. Roithová, *Angew. Chem.* **2006**, *118*, 5835; *Angew. Chem. Int. Ed.* **2006**, *45*, 5705; j) M. Brönstrup, D. Schröder, I. Kretzschmar, H. Schwarz, J. N. Harvey, *J. Am. Chem. Soc.* **2001**, *123*, 142; k) A. Fiedler, I. Kretzschmar, D. Schröder, H. Schwarz, *J. Am. Chem. Soc.* **1996**, *118*, 9941.
[14] M. B. Comisarow, V. Grassi, G. Parisod, *Chem. Phys. Lett.* **1978**, *57*, 413.
[15] M. Schlangen, D. Schröder, H. Schwarz, *Helv. Chim. Acta* **2005**, *88*, 1405.
[16] T. Su, M. T. Bowers, *J. Chem. Phys.* **1973**, *58*, 3027.
[17] a) K. Eller, W. Zummack, H. Schwarz, *J. Am. Chem. Soc.* **1990**, *112*, 621; b) K. Eller, H. Schwarz, *Int. J. Mass Spectrom. Ion Processes* **1989**, *93*, 243.
[18] D. Schröder, H. Schwarz, D. E. Clemmer, Y. Chen, P. B. Armentrout, V. I. Baranov, D. K. Böhme, *Int. J. Mass Spectrom. Ion Processes* **1997**, *161*, 175.
[19] Gaussian 09 (Revision A.02), M. J. Frisch, et al., Gaussian, Inc., Wallingford CT, **2009**.
[20] a) A. D. Becke, *J. Chem. Phys.* **1993**, *98*, 5648; b) A. D. Becke, *Phys. Rev. A* **1988**, *38*, 3098; c) C. T. Lee, W. T. Yang, R. G. Parr, *Phys. Rev. B* **1988**, *37*, 785.
[21] W. Kohn, L. J. Sham, *Phys. Rev.* **1965**, *140*, A1133.
[22] A. Schafer, C. Huber, R. Ahlrichs, *J. Chem. Phys.* **1994**, *100*, 5829.
[23] Z.-C. Wang, N. Dietl, R. Kretschmer, T. Weiske, M. Schlangen, H. Schwarz, *Angew. Chem.* **2011**, *123*, 12559; *Angew. Chem. Int. Ed.* **2011**, *50*, 12351.
[24] Z. C. Wang, X. N. Wu, Y. X. Zhao, J. B. Ma, X. L. Ding, S. G. He, *Chem. Eur. J.* **2011**, *17*, 3449.
[25] H. B. Schlegel, *J. Comput. Chem.* **1982**, *3*, 214.
[26] C. Peng, P. Y. Ayala, H. B. Schlegel, M. J. Frisch, *J. Comput. Chem.* **1996**, *17*, 49.
[27] a) D. G. Truhlar, M. S. Gordon, *Science* **1990**, *249*, 491; b) C. Gonzalez, H. B. Schlegel, *J. Phys. Chem.* **1990**, *94*, 5523; c) C. Gonzalez, H. B. Schlegel, *J. Chem. Phys.* **1989**, *90*, 2154; d) K. Fukui, *Acc. Chem. Res.* **1981**, *14*, 363; e) K. Fukui, *J. Phys. Chem.* **1970**, *74*, 4161.

